Latent Dataset Distillation with Diffusion Models

Brian B. Moser^{1,2,3}, Federico Raue^{1,3}, Sebastian Palacio¹, Stanislav Frolov^{1,2}, and Andreas Dengel^{1,2}

German Research Center for Artificial Intelligence (DFKI), Germany RPTU Kaiserslautern-Landau, Germany Equal Contribution first.second@dfki.de

Abstract. The efficacy of machine learning has traditionally relied on the availability of increasingly larger datasets. However, large datasets pose storage challenges and contain non-influential samples, which could be ignored during training without impacting the final accuracy of the model. In response to these limitations, the concept of distilling the information on a dataset into a condensed set of (synthetic) samples, namely a distilled dataset, emerged. One crucial aspect is the selected architecture (usually ConvNet) for linking the original and synthetic datasets. However, the final accuracy is lower if the employed model architecture differs from the model used during distillation. Another challenge is the generation of high-resolution images, e.g., 128x128 and higher. In this paper, we propose Latent Dataset Distillation with Diffusion Models (LD3M) that combine diffusion in latent space with dataset distillation to tackle both challenges. LD3M incorporates a novel diffusion process tailored for dataset distillation, which improves the gradient norms for learning synthetic images. By adjusting the number of diffusion steps, LD3M also offers a straightforward way of controlling the trade-off between speed and accuracy. We evaluate our approach in several ImageNet subsets and for high-resolution images (128x128 and 256x256). As a result, LD3M consistently outperforms state-of-the-art distillation techniques by up to 4.8 p.p. and 4.2 p.p. for 1 and 10 images per class, respectively.

1 Introduction

The undeniable success of employing larger datasets has led to a growing body of research [4, 8, 16, 53, 54, 61] trying to solve the question: Is the large-scale size of a dataset essential for training models capable of solving complex visual tasks? Using large-scale datasets to train modern neural networks demands special equipment and infrastructure. It further poses challenges regarding storing and data pre-processing [20]. Moreover, recent studies have shown that even popular large-scale datasets contain non-influential samples, which could be ignored during training without impacting the final model [31]. These insights led to methods that try to decrease the magnitude of training sets, e.g., importance sampling and coreset selection [10, 23, 39, 41].

Following the idea of knowledge distillation [25], dataset distillation [63] aims to generate a small set of representative synthetic samples from the original training set. Since then, the idea of condensing large datasets into a few synthesized images, e.g., one image per class, without significantly compromising training, has rapidly gained traction. It has found applications in the privacy domain or accelerated neural architecture search [7, 14, 38, 60].

However, conventional methods for dataset distillation like Dataset Condensation [69], Distribution Matching [68], and Matching Training Trajectories [6] still face major limitations. The core problems are the generalization across architectures and high image resolutions, i.e. 128×128 or 256×256 . For instance, models show peak performance when their architecture matches the one used for distillation. However, the performance deteriorates if other architectures are applied. These challenges arise primarily from the common practice of distilling the raw pixel values of synthetic images [8]. Optimizing pixels directly leads to datasets that overfit the network that is used during the dataset distillation [3].

To address these challenges, we propose Latent Dataset Distillation with Diffusion Models (LD3M), which integrates state-of-the-art image generation methods with dataset distillation. LD3M avoids distilling into the input space and finds better representations in latent space that can be decoded into synthetic samples. Training multiple architectures with the synthetic samples leads to higher accuracy overall, addressing the lack of generalization w.r.t. traditional distillation methods. The consistency of the latent space also leads to improved quality of high-resolution samples compared to other state-of-the-art methods.

One benefit of LD3M is that it exploits a pre-trained diffusion model out of the box. Moreover, LD3M is compatible on top of any distillation algorithm, turning LD3M into a flexible and more powerful alternative to raw distillation methods [6,68,69]. The general formulation of LD3M enables the use of any diffusion model, making it extensible to new developments in the field of diffusion models. Also, using the pre-trained LDM allows for a straightforward initialization of the distilled dataset. In other words, the original images are passed through the encoder to obtain their respective latent codes. This is an advantage over current latent distillation methods that use costly GAN inversions [5,71].

We evaluate our approach using varying numbers of images per class, multiple model architectures, and varying image resolutions, all in the context of image classification. Our results show that LD3M is faster in distillation and generates datasets leading to higher accuracy on various architectures than the state-of-the-art method GLaD [58]. Overall, our paper:

- introduces LD3M as a latent distillation method with pre-trained diffusion models bridging latent and synthetic images. LD3M can be used out of the box with existing dataset distillation methods.
- provides an alternative and straightforward diffusion process suitable for dataset distillation. LD3M lays the groundwork for future research and is easily extendable to new diffusion models.
- improves performance compared to the state-of-the-art method GLaD on various dataset distillation experiments.

2 Background

Parts of L3DM rely on different methods, including more primitive distillation algorithms. In this section, we briefly review the most important and discuss their relation to our method.

2.1 Dataset Distillation Algorithms for Image Classification

Distillation algorithms compress training image datasets into a small set of synthetic samples, whose size is defined by the number of Images Per Class (IPC). The synthetic images are learnable, similar to weights in neural networks. After termination of the distillation algorithm, the synthetic images constitute an expressive representation of a class in the original dataset. Most approaches initialize the synthetic images with IPC-many random images from each class as a starting point. The core idea is to use a simple ConvNet and align its training progress on the synthetic set with the progress on the original dataset [32,36,67]. This alignment can be expressed as an optimization process that updates the synthetic images in order to maximize training progress similarity. In this section, we describe three commonly used methods, namely Dataset Condensation [69], Distribution Matching [68], and Matching Training Trajectories [6]. Each method represents a different type of distillation algorithm: gradient matching, feature matching, and parameter matching.

Dataset Condensation (DC) ensures the alignment by deriving the gradients via a classification error [69]. It calculates the loss on real and the respective synthetic data. Next, it minimizes the distance between the two loss gradients.

Distribution Matching (DM) obtains gradients by minimizing the produced features on the real and synthetic datasets. It enforces the feature extractor (ConvNet) to produce similar features for real and synthetic images [68].

Matching Training Trajectories (MTT) does not rely on the gradients obtained by calculating the classification error or the feature distance. Instead, it uses the network parameters [6]. It trains many model instantiations on the original dataset, called experts, and records the history of parameters at predetermined intervals, called expert trajectories. For dataset distillation, it samples a random set of parameters from this history at a given timestamp and trains a new network initialized with the parameters on the respective synthetic images. Finally, it minimizes the distance between the trajectory on the real dataset and the trajectory on the synthetic one. As a result, it tries to mimic the training path (trajectory of parameters) of the original dataset with the synthetic images.

2.2 Diffusion Models for Image Generation

The premise of diffusion models is to generate real-looking data by progressively adding noise to an initial sample and subsequently reversing the process by eliminating the noise. This reversal aids in approximating a complex target data distribution gradually. [42, 43, 65]. The main characteristic of diffusion models, which sets them apart from previous generative models, is their dependency

on previous time steps. Through iterative refinement, a generative model keeps track of small perturbations and corrects them instead of predicting a large and challenging transformation [26, 50, 65]. These iterative steps unfold forward and backward in time. The distinct stages of the diffusion process are characterized as follows:

Forward Diffusion - The original input data is progressively degraded by adding noise, moving forward in time.

Backward Diffusion - This stage involves the iterative denoising of the previously degraded data, effectively reversing the noise addition process and thus moving backward in time.

To reduce the computational requirements for generating high-resolution images, Rombach et al. propose to move the diffusion process towards the latent space representations of an autoencoder structure, which they called Latent Diffusion Model (LDM) [55]. Usually, a pre-trained autoencoder [18] is used to compress input data into a low-dimensional latent representation. Next, LDM uses the regular diffusion pipeline in the latent space and employs a decoder to translate the result, the diffusion-processed latent code, back to pixel space.

This application of the diffusion pipeline in latent space is essential for LD3M, as we want to optimize the latent codes that generate the synthetic images. Thus, LD3M directly exploits two main components of the LDM during dataset distillation: The denoising U-Net and the decoder to translate the latent code to image space. The encoder and embedding network for the conditioning will be used once to instantiate the initial latent and conditioning codes for each class.

2.3 Dataset Distillation with Generative Models

The Generative Latent Distillation (GLaD) incorporates a deep generative prior to the distillation process, serving as a form of regularization [8]. This is achieved by optimizing the latent codes of a pre-trained generative model instead of directly focusing on the raw pixel values. GLaD uses StyleGAN-XL [58], a large-scale GAN, and an adaptation of StyleGAN3 [29] as the pre-trained generator.

Like most distillation methods, it initializes its synthetic images with latent representations of real images. The process of distilling the latent space representation of an image in StyleGAN-XL is similar to a pseudo-inversion task, connecting to the broader research domain of GAN inversion [5,71]. The central concept involves mapping an actual input image into GAN latent codes, where selecting a particular latent space balances expressiveness and reconstruction fidelity, as evidenced in prior research [62,73]. The authors discovered that distilling into even the more expansive \mathbf{W}^+ latent space [1], which is among the most flexible in traditional StyleGAN inversion contexts, proved overly constraining. This approach limited synthetic samples to realistic pre-trained images. However, unlike real image inversion, synthetic samples do not necessitate realism. As a result, the authors utilized "Fn" spaces, an alternative method to allow a more diverse and flexible set of images generated by the latent codes [52, 72]. This technique focuses on refining the latent representation of the n-th hidden

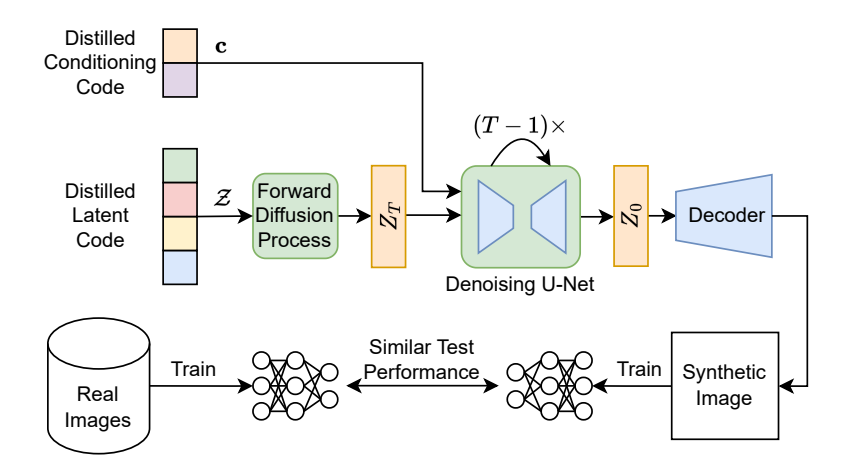


Fig. 1: Overview of the LD3M framework. Two components influence the generation of the synthetic images: The distilled latent codes and the distilled conditioning codes. The distilled latent codes are perturbated via Gaussian noise to the initial state \mathbf{z}_T . Next, it is iteratively denoised (T-1) times with the pre-trained denoising U-Net of the LDM. Within each computation of the intermediate state \mathbf{z}_t , we add a linearly decreasing influence of \mathbf{z}_T to allow an enhanced gradient flow to the distilled latent codes while making the conditioning also learnable. The pre-trained decoder translates the final latent code \mathbf{z}_0 back to pixel space. Note that LD3M can be used with any existing distillation algorithm, e.g., DC, DM, or MTT.

layer within the Style GAN-XL's "synthesis" network and concurrently adjusting all subsequent \mathbf{W}^+ modulation codes.

3 LD3M

In this work, we introduce a novel method called Latent Dataset Distillation with Diffusion Models (LD3M) that leverages the generative power of diffusion models for high-resolution image generation. Our work focuses on dataset distillation in the latent space of diffusion models to solve the generalization problem of unseen architectures and high-resolution images (i.e., 256x256). In more detail, we exploit a pre-trained Latent Diffusion Model (LDM) that maps the latent space to image space without fine-tuning [44,55,65]. Since LDM is a conditional diffusion model, the generative process contains two crucial elements: the latent codes and their associated conditioning code. Therefore, the challenge is to find the latent code and the conditioning code to generate the distilled dataset. In the following, we will explain the sampling process, which takes the latent and conditioning code as input and generates the synthetic image. Next, we describe how we initialize the latent codes before dataset distillation and, finally, how we use gradient checkpointing to save VRAM. A general overview of our approach is shown in Figure 1.

3.1 Sampling Process

We use a pre-trained LDM without fine-tuning. Thus, we focus primarily on the backward diffusion process p, which starts from initial state \mathbf{z}_T , usually Gaussian noise $\varepsilon \in \mathcal{N}(\mathbf{0}, \mathbf{I})$, and performs the inference conditioned on \mathbf{c} , which is in our case the pre-trained embedding of the class label [44,65]. The forward diffusion process is only needed to derive \mathbf{z}_T from the learned and distilled latent representations \mathcal{Z} . Therefore, we can view \mathbf{z}_T as the distorted representation of \mathcal{Z} , which the LDM refines. We approximate p with a parameterized time-conditional process p_{θ} , such that

$$p_{\theta}(\mathbf{z}_{0:T}|\mathbf{c}) = p(\mathbf{z}_T) \prod_{t=1}^{T} p_{\theta}(\mathbf{z}_{t-1}|\mathbf{z}_t, \mathbf{c})$$
(1)

$$p(\mathbf{z}_T) = \mathcal{N}(\mathbf{z}_T \mid \mathbf{0}, \mathbf{I}) \tag{2}$$

$$p_{\theta}(\mathbf{z}_{t-1}|\mathbf{z}_t, \mathbf{c}) = \mathcal{N}(\mathbf{z}_{t-1} \mid \mu_{\theta}(\mathbf{c}, \mathbf{z}_t, \gamma_t), \sigma_t^2 \mathbf{I}). \tag{3}$$

As standard in the literature [35,57], we predict the parameterized mean by subtracting the scaled noise between two subsequent time steps with

$$\mu_{\theta}(\mathbf{c}, \mathbf{z}_{t}, \gamma_{t}) = \frac{1}{\sqrt{\alpha_{t}}} \left(\mathbf{z}_{t} - \frac{1 - \alpha_{t}}{\sqrt{1 - \gamma_{t}}} f_{\theta}(\mathbf{c}, \mathbf{z}_{t}, \gamma_{t}) \right), \tag{4}$$

where $f_{\theta}(\mathbf{c}, \mathbf{z}_t, \gamma_t)$ is the noise prediction of ε_t with a time-conditional U-Net at time step t. Together with the variance σ_t^2 , we can calculate the subsequent state \mathbf{z}_{t-1} via

$$\mathbf{z}_{t-1} \leftarrow \mu_{\theta}(\mathbf{c}, \mathbf{z}_t, \gamma_t) + \sigma_t^2 \varepsilon_t.$$
 (5)

For dataset distillation, we make the embedded conditioning \mathbf{c} as well as the latent code \mathcal{Z} leading to the initial state \mathbf{z}_T learnable. Since the LDM is not trained from scratch, only modifying the condition state \mathbf{c} is insufficient and does not allow the LDM enough freedom to generate expressive synthetic images, which necessitates the need to make \mathcal{Z} learnable [34, 51]. We will show this quantitatively in the experiments section. The initial experiments indicate that making only the conditioning \mathbf{c} of the LDM learnable predominantly produces images resembling real data.

A significant challenge in making the latent code \mathcal{Z} , which leads to the initial state \mathbf{z}_T , learnable arises from the numerous time steps during the backward diffusion process. For instance, LDM employs T=200 steps during training. This extensive computation chain leads to vanishing gradients for \mathbf{z}_T , impeding the effective distillation of synthetic images [27]. We modify Equation 5 to counteract this by including residual connections in the computational graph, thereby enhancing gradient flow. Specifically, we integrate the initial state \mathbf{z}_T into the computation of the intermediate states \mathbf{z}_t . Additionally, we systematically diminish its influence as t approaches 0. This adjustment ensures an enhanced propagation of gradients in the computational graph, crucial for the generation of diverse and representative synthetic latent codes \mathcal{Z} :

$$\mathbf{z}_{t-1} \leftarrow \left((1 - \frac{t}{T}) \cdot \mu_{\theta}(\mathbf{c}, \mathbf{z}_t, \gamma_t) + \frac{t}{T} \cdot \mathbf{z}_T \right) + \sigma_t^2 \varepsilon_t.$$
 (6)

Note that this reformulation is not bound to LDMs and can be used by any diffusion model type for future work.

3.2 Initializing Latent Codes

We initialize the synthetic images with random pictures representing the respective class. More specifically, we derive the latent codes leading to the selected random images. We share this challenge with GLaD, which uses StyleGAN-XL before applying dataset distillation algorithms. GLaD uses GAN-inversion techniques to solve this problem, which is time-consuming. To obtain the latent code for a GAN, one has to solve the optimization problem $\mathcal{Z}^* = \arg\min_{\mathcal{Z}} \mathcal{L}(y, G(\mathcal{Z}))$. A solution can be optimization-based, learning-based, or hybrid-based, which needs careful adjustment and testing [8,64]. Nonetheless, the solutions are time-consuming as they iteratively sample possible \mathcal{Z}^* or require extra training.

In contrast, LD3M can initialize the latent codes straightforwardly by applying the pre-trained encoder to the random images. Furthermore, LD3M initializes the embedded condition information by applying the pre-trained embedding network. As a result, initialization with LD3M is more straightforward than GLaD and omits careful adjustments before applying dataset distillation.

3.3 Memory Saving via Checkpointing

Due to the substantial VRAM requirements for the forward pass in modern generative models, a straightforward implementation is not feasible with limited GPUs [20]. Therefore, as in GLaD [8], we employ gradient checkpointing [9].

At each distillation iteration, we generate the synthetic images $\mathcal{S} = G(\mathcal{Z})$ without gradients. Then, we calculate the distillation loss \mathcal{L} and the gradients for the synthetic images $(\partial \mathcal{L}/\partial \mathcal{S})$. Next, we delete the computation graph and its gradient. To compute $\partial \mathcal{L}/\partial \mathcal{Z}$, we recompute the forward pass through G, $\mathcal{S} = G(\mathcal{Z})$, this time tracking gradients such to obtain $\partial \mathcal{S}/\partial \mathcal{Z}$. The application of the chain rule delivers $\partial \mathcal{L}/\partial \mathcal{Z} = (\partial \mathcal{L}/\partial \mathcal{S})(\partial \mathcal{S}/\partial \mathcal{Z})$ which is used to update the latent codes and the conditioning.

Since our generative model G applies multiple diffusion steps, we also employ checkpointing within $G(\mathcal{Z})$ for each noise prediction ϵ_t of the U-Net. It saves $\partial \mathbf{z}_t/\partial \mathbf{z}_{t+1}$. The application of the chain rule leads to

$$\partial \mathcal{L}/\partial \mathcal{Z} = (\partial \mathcal{L}/\partial \mathbf{z}_0) \cdot \prod_{t=1}^{T} \frac{\partial \mathbf{z}_{t-1}}{\partial \mathbf{z}_t} \cdot (\partial \mathbf{z}_T/\partial \mathcal{Z})$$
 (7)

Similarly, the condition information \mathbf{c} is derived by

$$\partial \mathcal{L}/\partial \mathbf{c} = (\partial \mathcal{L}/\partial \mathbf{z}_0) \cdot \prod_{t=1}^{T} \frac{\partial \mathbf{z}_{t-1}}{\partial \mathbf{z}_t} \cdot (\partial \mathbf{z}_T/\partial \mathbf{c})$$
 (8)

4 Experiments

We follow a similar setup as Cazenavette et al. [8]. Thus, we evaluate the cross-architecture performance for IPC=1 (MTT, DC, DM) and IP=10 (DC, DM) with image size 128×128 . Moreover, we run a high-resolution dataset distillation evaluation with DC and image size 256×256 for IPC=1. Finally, we compare the results visually with GLaD and analyze the impact of time steps and different components of LD3M. We maintain a consistent set of hyper-parameters across experiments to guarantee a fair comparison. See supplementary materials for more details.

4.1 Setup

Datasets. We evaluate the mean and standard deviation of the accuracy on 10-class subsets of ImageNet-1k [12]. The 10-class subsets were derived from previous dataset distillation work, i.e. ImageNet-Birds, ImageNet-Fruits, and ImageNet-Cats [6]. In addition, we employ two other commonly used subsets, namely ImageNette and ImageWoof [28]. Lastly, the remaining used subsets are based on the evaluation performance of a ResNet-50 model (pre-trained on ImageNet) [8]. These subsets are ImageNet-A, consisting of the top-10 classes; ImageNet-B, consisting of the next 10 and so on for ImageNet-C, ImageNet-D, and ImageNet-E. More details can be found in the supplementary materials.

Evaluation Protocol. We first distill synthetic datasets using the designated algorithms and then assess the quality of the datasets by measuring the performance across unseen network architectures. To evaluate a synthetic dataset with a specific architecture, we train a new network from scratch on the distilled dataset and subsequently test its performance on the validation set. The training protocol is consistent across all networks and datasets for fair comparison. Each architecture employs a predetermined and constant initial learning rate. This entire process is replicated five times, with the report including the mean validation accuracy plus or minus one standard deviation.

Network Architectures. As in GLaD [8] and prior dataset distillation work [11,48,49], we use the ConvNet-5 and ConvNet-6 architecture to distill the 128×128 and 256×256 datasets, respectively [21]. Similarly, we use AlexNet [33], VGG-11 [59], ResNet-18 [24], and a Vision Transformer [15] for evaluating unseen architectures.

Latent Diffusion Model. For the diffusion model, we use the ImageNet pretrained LDM [55], which guarantees a fair comparison with the ImageNet pretrained StyleGAN-XL used in GLaD [8]. We use the pre-trained autoencoder with $2\times$ compression of the LDM without further adjustments to compress into and decompress out of the latent space. We employ for all experiments a max. time step T=10 for image size 128×128 and T=20 for 256×256 . Besides this hyper-parameter, no adjustment to the pre-trained LDM was necessary.

Table 1: Cross-architecture performance with 1 image per class on all ImageNet (128×128) subsets. We used the unseen architectures AlexNet, VGG11, ResNet18, and ViT. The average performance of these models was then evaluated on actual validation sets. Using LDM as a deep generative prior markedly enhanced the ability of all tested methods to generalize across various architectures in all the datasets examined. In 9 out of 10 subsets (marked with blue), LD3M reaches the best overall performance. The best performance within one distillation algorithm is marked in bold in each subset, primarily achieved by LD3M.

Distil. Space	Alg.	ImNet-A	ImNet-B	ImNet-C	ImNet-D	$\operatorname{ImNet-E}$	ImNette	ImWoof	ImNet-Birds	ImNet-Fruits	ImNet-Cats
	MTT	33.4 ± 1.5	34.0±3.4	31.4±3.4	27.7±2.7	24.9 ± 1.8	24.1±1.8	16.0 ± 1.2	25.5 ± 3.0	18.3 ± 2.3	18.7±1.5
Pixel	DC	$38.7 {\pm} 4.2$	38.7 ± 1.0	33.3 ± 1.9	26.4 ± 1.1	27.4 ± 0.9	28.2 ± 1.4	17.4 ± 1.2	28.5 ± 1.4	20.4 ± 1.5	19.8 ± 0.9
	$_{\mathrm{DM}}$	$27.2 {\pm} 1.2$	24.4 ± 1.1	$23.0 \!\pm\! 1.4$	$18.4{\pm}0.7$	$17.7{\pm}0.9$	20.6 ± 0.7	$14.5{\pm}0.9$	17.8 ± 0.8	14.5 ± 1.1	14.0 ± 1.1
	MTT	39.9 ± 1.2	39.4±1.3	34.9 ±1.1	30.4 ± 1.5	29.0 ± 1.1	30.4 ± 1.5	17.1 ± 1.1	28.2 ± 1.1	21.1 ± 1.2	19.6 ± 1.2
GLaD	DC	41.8 ± 1.7	42.1 ± 1.2	35.8 ± 1.4	28.0 ± 0.8	29.3 ± 1.3	31.0 ± 1.6	17.8 ± 1.1	29.1 ± 1.0	22.3 ± 1.6	21.2 ± 1.4
	$_{\mathrm{DM}}$	$31.6 {\pm} 1.4$	31.3 ± 3.9	26.9 ± 1.2	$21.5{\pm}1.0$	$20.4{\pm}0.8$	$21.9{\pm}1.1$	$15.2{\pm}0.9$	18.2 ± 1.0	20.4 ± 1.6	16.1 ± 0.7
	MTT	40.9 ±1.1	41.6 ±1.7	34.1 ± 1.7	31.5 ± 1.2	30.1 ± 1.3	32.0 ± 1.3	$\textbf{19.9} {\pm} 1.2$	$\textbf{30.4} {\pm} 1.5$	21.4 ± 1.1	$22.1{\pm}1.0$
LD3M	DC	42.3 ± 1.3	42.0 ± 1.1	37.1 ± 1.8	29.7 ± 1.3	31.4 ± 1.1	$\textbf{32.9} \!\pm\! 1.2$	18.9 ± 0.6	30.2 ± 1.4	22.6 ± 1.3	21.7 ± 0.8
	DM	35.8 ± 1.1	34.1 ± 1.0	30.3 ± 1.2	24.7 ± 1.0	24.5 ± 0.9	26.8 ± 1.7	18.1 ± 0.7	23.0 ± 1.8	$24.5{\pm}1.9$	17.0 ± 1.1

Table 2: Cross-architecture performance with 10 images per class on the subsets ImageNet A to E. LD3M (marked with blue) achieved the best performance per subset. The best performance within one distillation algorithm is marked in bold in each subset, primarily achieved by LD3M.

Distil. Space	Alg.	All	ImNet-A	ImNet-B	ImNet-C	ImNet-D	ImNet-E
Pixel	DC	42.3 ± 3.5	52.3 ± 0.7	45.1 ± 8.3	40.1 ± 7.6	36.1 ± 0.4	38.1±0.4
Fixei	DM	$44.4 {\pm} 0.5$	52.6 ± 0.4	50.6 ± 0.5	47.5 ± 0.7	$35.4{\pm}0.4$	36.0 ± 0.5
GLaD	DC	45.9 ± 1.0	53.1 ± 1.4	50.1 ± 0.6	48.9 ± 1.1	38.9 ± 1.0	38.4 ± 0.7
GLaD	DM	$45.8{\pm}0.6$	52.8 ± 1.0	$51.3{\pm}0.6$	$\boldsymbol{49.7} {\pm} 0.4$	$36.4{\pm}0.4$	38.6 ± 0.7
LD3M	DC	47.1±1.2	55.2±1.0	51.8±1.4	49.9±1.3	39.5±1.0	39.0±1.3
LD3M	DM	47.3 ± 2.1	$\textbf{57.0} {\pm} \textbf{1.3}$	$\textbf{52.3} {\pm} \textbf{1.1}$	48.2 ± 4.9	$\textbf{39.5} {\pm} \textbf{1.5}$	$\textbf{39.4} {\pm} \textbf{1.8}$

4.2 Results

Cross-Architecture Evaluation, IPC=1. Our method LD3M consistently surpasses the performance of GLaD on unseen architectures for IPC=1 (see Table 1). Following [8], we test all ten aforementioned subsets of ImageNet and apply the distillation algorithms MTT, DC, and DM. The enhanced performance of our LD3M is consistent across most subsets, except for slight deviations in MTT on ImageNet-C and DC on ImageNet-B. Notably, these exceptions still closely align with the original performance metrics and fall within the standard deviation range, underlining the robustness of our approach. The enhancement in performance is most pronounced when employing the DM distillation algorithm. LD3M with LDM outperforms its GAN-based GLaD counterpart by approximately four p.p. across most subsets. This significant improvement underscores the effectiveness of LDMs in capturing complex data distributions in synthetic

Table 3: 256×256 distilled HR images using the DC distillation algorithm and IPC=1. For both scenarios (LDM and GAN), we evaluate pre-trained generators on ImageNet [12], FFHQ [30], and randomly initialized. The best overall performance for each subset is marked in bold; the top 3 performances are in blue.

Distillation Space	All	ImNet-A	ImNet-B	ImNet-C	ImNet-D	ImNet-E
Pixel	29.5 ± 3.1	38.3 ± 4.7	32.8 ± 4.1	27.6 ± 3.3	25.5 ± 1.2	23.5 ± 2.4
GLaD (ImageNet) GLaD (Random) GLaD (FFHQ)	$34.5 {\pm} 1.6$	37.4 ± 5.5 39.3 ± 2.0 38.3 ± 5.2	$40.3{\pm}1.7$	$35.0{\pm}1.7$	$27.9{\pm}1.4$	$29.8{\pm}1.4$
LD3M (ImageNet) LD3M (Random) LD3M (FFHQ)	36.5 ± 1.6		$41.9 {\pm} 1.7$	37.1 ± 1.4	$30.5{\pm}1.5$	31.1±1.4



Fig. 2: Visual comparison of LD3M versus GLaD for 1000 iterations with MTT on ImageNette. LD3M produces more abstract and contrast-richer synthetic images.

images more effectively than StyleGAN-XL in HR image distillation and further improves the gap between pixel-based and latent-based dataset distillation.

Cross-Architecture Evaluation, IPC=10. Further supporting our findings, Table 2 illustrates the superior performance of LD3M over GLaD in scenarios with IPC=10 using the distillation algorithms DC and DM on ImageNet A to E. The trend observed is similar to the IPC=1 scenario, with LD3M demonstrating a clear advantage over GLaD. The exception of DM on ImageNet-C is marginal and still outperforms pixel-based distillation, but also shows that the application of LDM for IPC=10 has the most significant improvements in DM compared to DC, e.g., ca. 4 p.p. improvement on ImageNet-A. LD3M reaches an overall average accuracy of 47.08 % with DC and 47.28 % with DM compared to 45.88 % and 45.76 % of GLaD with StyleGAN-XL. This experiment highlights the consistency and reliability of the LDM approach across different settings.

High-Resolution Distillation. In the context of 256×256 data, as shown in Table 3, a similar pattern of improved performance is evident. LD3M achieved all top-3 results per subset. To explore the versatility of LDMs, we experimented with various training configurations, including models pre-trained on ImageNet, FFHQ, and a randomly initialized model. Consistent with the find-

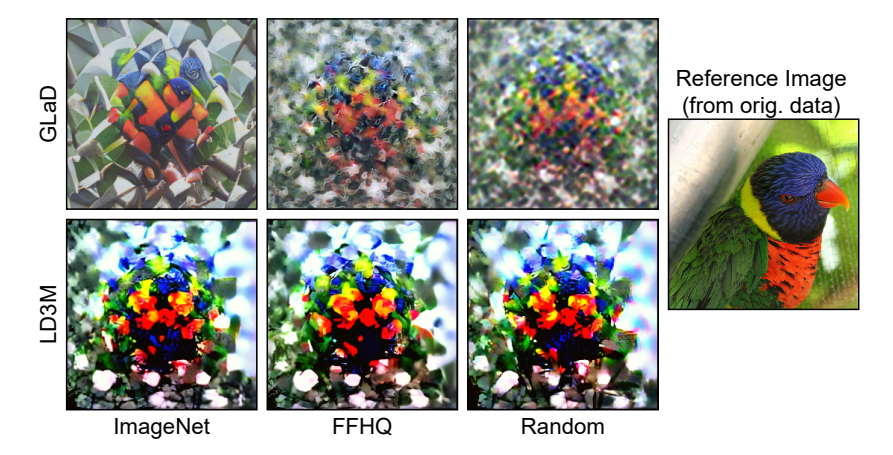


Fig. 3: Example 256×256 images of a distilled class (ImageNet-B: Lorikeet) with differently initialized GLaD and LD3M. Initializations are denoted at the bottom.

ings using GANs, these varied LDM configurations demonstrated improved cross-architectural generalization compared to direct pixel-space distillation.

Visual Comparison. As presented in Figure 2, visual comparisons depict the results of GLaD and the LD3M. These comparisons reveal that the generated images by LD3M are notably more abstract and exhibit higher contrast than those produced by GLaD. While GLaD tends to generate images more closely resembling the initial real image used in the latent code representation, LD3M diverges towards a more stylized and vivid visual representation. This highlights a more flexible learning space for dataset distillation algorithms.

Figure 3 shows high-resolution distillation (256×256) under different initializations. Again, LD3M produces notably more abstract images with higher contrast. Surprisingly, LD3M generates more stable images under different initializations, as GLaD's generated images vary more. GLaD's generation becomes more noisy towards random initialization (see from left to right). Additional visualizations for qualitative examination of all other experiments are provided in the supplemental materials of this work.

Diffusion Time Steps Analysis. Our investigation into the trade-off between the runtime and accuracy of distilled datasets is shown in Figure 4. It illustrates the diffusion steps versus the accuracy of our LDM-based distillation method across different maximum time steps T in the diffusion process, specifically evaluated on the ImageNet A-E datasets using the MTT algorithm. There is a notable increase in accuracy for setting the maximum time step up to 40 for the diffusion process. However, as we progress beyond 40 time steps, performance is significantly declining. An example is shown in Figure 5 for the freight car class from ImageNet-C. This decline could be attributed to vanishing gradients during the diffusion process, suggesting that strategies other than the linear addition of the initial state could avoid the performance decline.

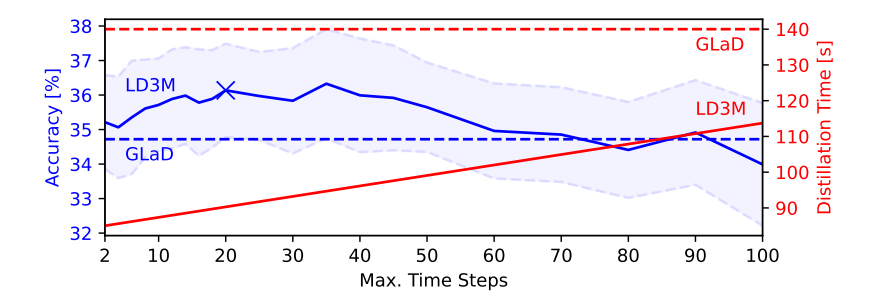


Fig. 4: Distilled dataset performance (average of ImageNet A-E via MTT and IPC=1) for different max. time steps employed in the diffusion process with mean and standard deviation (light blue dotted). It illustrates the trade-off between runtime and accuracy over increasing time steps. LD3M shows improved performance for the first 40 time steps, while the performance deteriorates for greater time steps. GLaD needs around 140 seconds per iteration on the same hardware (NVIDIA RTX3090) with 34.72 % average accuracy, shown as dotted lines. Best trade-off marked with "X".

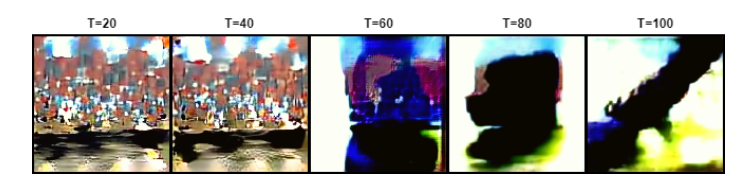


Fig. 5: Example images of a distilled class (Freight Car) for different time steps settings. We observe that distillation can collapse for higher time step settings (see the three images on the right).

However, if the same pre-trained LDM is applied, we do not expect other strategies to improve the overall reachable image quality significantly. The ability to tailor the diffusion process according to specific accuracy and runtime opens up new possibilities for dataset distillation across various computational settings. It allows for strategically allocating computational resources, ensuring the models are accurate and practically viable for real-world applications.

Ablation Study. In our initial experiments, we evaluated the impact of incorporating different aspects of the LDM, as described in our methodology section and shown in Table 4. We used LD3M on ImageNette and MTT for 1,000 distillation steps and an Image Per Class (IPC) of 1. We also compared against GLaD and evaluated the results with unseen architectures. By applying only learnable conditioning, the resulting performance of LD3M is just roughly five p.p. above random chance. However, the real breakthrough was observed when we allowed the latent representation within the LD3M to be learnable. This adjustment significantly improved accuracy across all models but still lagged behind those achieved with GLaD. Another enhancement was implementing the modified formula for calculating the intermediate states \mathbf{z}_t in the LDM. This

Table 4: Comparison of different LDM variations with MTT on ImageNette for 1,000 distillation steps and IPC=1. Tested were the distillation of the LDM by making only the conditioning learnable, one LDM with also learnable initial latent representation (\mathbf{z}_T), and lastly, one LDM which incorporates the initial latent representation in the calculation of intermediate latent states (see Equation 6).

Method	All	AlexNet	VGG-11	ResNet-18	ViT
GLaD	26.6 ± 1.6	28.7 ± 0.3	$29.2 {\pm} 1.2$	30.8 ±2.9	17.8 ± 1.5
LDM learn. conditioning (c)	15.8 ± 1.5	14.2 ± 2.6	15.1 ± 1.6	$16.5 {\pm} 4.9$	16.8 ± 4.0
$+$ learn. latent (\mathbf{z}_T)	22.3 ± 2.0	22.8 ± 2.0	$26.3 {\pm} 0.9$	23.4 ± 3.2	17.5 ± 2.0
+ interpolation (Eq. 6)	$28.1 {\pm} 3.3$	29.2 ± 1.9	$29.2 {\pm} 1.2$	30.6 ± 1.3	$\textbf{25.1} {\pm} 1.7$

involved incorporating the initial state \mathbf{z}_T into the calculation of intermediate states \mathbf{z}_t , enabling LD3M to surpass the GLaD performance.

To investigate the impact of the modified Equation 6, we measured the gradient norms of the latent code during distillation for both cases, with and without the incorporation of the initial state \mathbf{z}_T . The increase from the non-modified version to the modified version is approximately 66.87 %. This outcome emphasizes the importance of the modified formula for combating vanishing gradients.

5 Related Work

Diffusion Models vs GANs. In the study by Dhariwal et al., it was established that diffusion models exhibit superior performance in image generation tasks compared to GANs [13]. Since then, the concept of diffusion models disrupted various other related fields, such as image restoration [35, 40, 42, 56], layout-to-image [70], inpainting [37, 66], medical imaging [46, 47] and more [2, 44, 45, 65]. This development of the superior performance of diffusion models over GANs across various fields inspired this work. Unlike GANs, diffusion models do not require extensive regularization and optimization strategies to mitigate issues like optimization instability and mode collapse [19].

LDMs for GLaD. The closest work to ours is presented by Duan et al. [17], which uses the pre-trained autoencoder structure of the LDM to derive latent codes in GLaD. As a result, they also utilized the straightforward encoding strategy by applying the encoder to initial images. A notable distinction, however, lies in their lack of the diffusion process. Thus, they do not exploit the benefits of diffusion models, effectively limiting the capability of the generator to that of a basic autoencoder. Additionally, the experimental setup in their study diverges from the experiments established in GLaD, presenting challenges in conducting a direct and fair comparative analysis. For instance, they evaluate their approach with more latent codes per class (LPC), defined by how many latent vectors would have the same storage as one IPC, i.e., 12 LPC for IPC=1 or 120 LPC for IPC=10. Compared to our evaluation and that of GLaD, we have one latent code for one IPC.

Diffusion Models in Dataset Distillation. Another notable mention is the work of Gu. et al. [22], which proposed a Minimax Diffusion process for dataset distillation. While they present a promising hierarchical diffusion control mechanism to enable dataset distillation, it is another dataset distillation algorithm and, therefore, orthogonal to our work. Also, we enable a more straightforward mechanism by linearly adding the initial latent representation to enable distillation. For future work, we see great potential in using our method before applying the Minimax Diffusion process, as LD3M can be applied with any dataset distillation method.

6 Limitations

While LD3M improves dataset distillation compared to GLaD, it is essential to acknowledge certain limitations. A primary concern arises from the linear addition in the diffusion process (see Equation 6), which may not combat the vanishing gradient problem for larger time steps, as observed in our experiments [27]. Further alternative strategies for integrating the initial state \mathbf{z}_T in the diffusion process should be evaluated to address this issue, e.g., non-linear progress towards 0 as t approaches 0. These alternative approaches could offer more nuanced and dynamic ways to manage the influence of \mathbf{z}_T across different stages of the diffusion, potentially mitigating the problem of vanishing gradients and enhancing the overall efficacy of the distillation process.

7 Conclusion and Future Work

In this work, we introduced LD3M, a novel latent dataset distillation approach. LD3M benefits from the generative capabilities of diffusion models for synthesizing high-resolution images by introducing a modified formulation of the sampling process tailored for dataset distillation. Our results across diverse testing scenarios show that LD3M surpasses the state-of-the-art approach GLaD. In comparison, LD3M leads to enhanced image quality and faster distillation speed. Furthermore, LD3M allows fine-tuning the number of time steps to balance runtime and image quality. Moreover, the initialization of the latent code can be performed straightforwardly with the autoencoder applied to a random image of the respective class, which is an improvement over the GAN inversion necessary in GLaD. In conclusion, LD3M constitutes a transformative step in latent dataset distillation, broadening its applicability and enhancing its practicality.

For future work, other diffusion models should be investigated in LD3M, as well as alternative formulations to our modified equation (i.e., non-linear). Additionally, we will evaluate higher IPCs (e.g., 100, 200, 1000) and other scenarios such as Continual Learning and Privacy.

Acknowledgment

Will be updated...

References

- Abdal, R., Qin, Y., Wonka, P.: Image2stylegan: How to embed images into the stylegan latent space? In: Proceedings of the IEEE/CVF international conference on computer vision. pp. 4432–4441 (2019)
- 2. Bar-Tal, O., Yariv, L., Lipman, Y., Dekel, T.: Multidiffusion: Fusing diffusion paths for controlled image generation (2023)
- 3. Baradad Jurjo, M., Wulff, J., Wang, T., Isola, P., Torralba, A.: Learning to see by looking at noise. NeurIPS 34, 2556–2569 (2021)
- Bengio, S., Dembczynski, K., Joachims, T., Kloft, M., Varma, M.: Extreme classification (dagstuhl seminar 18291). In: Dagstuhl Reports. vol. 8. Schloss Dagstuhl-Leibniz-Zentrum fuer Informatik (2019)
- 5. Brock, A., Lim, T., Ritchie, J.M., Weston, N.: Neural photo editing with introspective adversarial networks. ICLR (2017)
- Cazenavette, G., Wang, T., Torralba, A., Efros, A.A., Zhu, J.Y.: Dataset distillation by matching training trajectories. In: CVPR (2022)
- 7. Cazenavette, G., Wang, T., Torralba, A., Efros, A.A., Zhu, J.Y.: Wearable imagenet: Synthesizing tileable textures via dataset distillation. In: CVPR (2022)
- 8. Cazenavette, G., Wang, T., Torralba, A., Efros, A.A., Zhu, J.Y.: Generalizing dataset distillation via deep generative prior. In: CVPR. pp. 3739–3748 (2023)
- Chen, T., Xu, B., Zhang, C., Guestrin, C.: Training deep nets with sublinear memory cost. arXiv preprint arXiv:1604.06174 (2016)
- Csiba, D., Richtárik, P.: Importance sampling for minibatches. The Journal of Machine Learning Research 19(1), 962–982 (2018)
- 11. Cui, J., Wang, R., Si, S., Hsieh, C.J.: Scaling up dataset distillation to imagenet-1k with constant memory. In: ICML (2023)
- 12. Deng, J., Dong, W., Socher, R., Li, L.J., Li, K., Fei-Fei, L.: Imagenet: A large-scale hierarchical image database. In: CVPR (2009)
- 13. Dhariwal, P., Nichol, A.: Diffusion models beat gans on image synthesis. Advances in neural information processing systems **34**, 8780–8794 (2021)
- 14. Dong, T., Zhao, B., Lyu, L.: Privacy for free: How does dataset condensation help privacy? In: ICML (2022)
- Dosovitskiy, A., Beyer, L., Kolesnikov, A., Weissenborn, D., Zhai, X., Unterthiner, T., Dehghani, M., Minderer, M., Heigold, G., Gelly, S., et al.: An image is worth 16x16 words: Transformers for image recognition at scale. ICLR (2020)
- 16. Driess, D., Xia, F., Sajjadi, M.S., Lynch, C., Chowdhery, A., Ichter, B., Wahid, A., Tompson, J., Vuong, Q., Yu, T., et al.: Palm-e: An embodied multimodal language model. arXiv preprint arXiv:2303.03378 (2023)
- 17. Duan, Y., Zhang, J., Zhang, L.: Dataset distillation in latent space. arXiv preprint arXiv:2311.15547 (2023)
- 18. Esser, P., Rombach, R., Ommer, B.: Taming transformers for high-resolution image synthesis. In: CVPR. pp. 12873–12883 (2021)
- 19. Frolov, S., Hinz, T., Raue, F., Hees, J., Dengel, A.: Adversarial text-to-image synthesis: A review. Neural Networks 144, 187–209 (2021)
- Ganguli, D., Hernandez, D., Lovitt, L., Askell, A., Bai, Y., Chen, A., Conerly, T., Dassarma, N., Drain, D., Elhage, N., et al.: Predictability and surprise in large generative models. In: 2022 ACM Conference on Fairness, Accountability, and Transparency (2022)
- Gidaris, S., Komodakis, N.: Dynamic few-shot visual learning without forgetting. In: CVPR (2018)

- Gu, J., Vahidian, S., Kungurtsev, V., Wang, H., Jiang, W., You, Y., Chen, Y.: Efficient dataset distillation via minimax diffusion. arXiv preprint arXiv:2311.15529 (2023)
- 23. Guo, C., Zhao, B., Bai, Y.: Deepcore: A comprehensive library for coreset selection in deep learning. In: International Conference on Database and Expert Systems Applications. pp. 181–195. Springer (2022)
- He, K., Zhang, X., Ren, S., Sun, J.: Deep residual learning for image recognition. In: CVPR (2016)
- Hinton, G., Vinyals, O., Dean, J.: Distilling the knowledge in a neural network. NeurIPS Workshop (2015)
- 26. Ho, J., Jain, A., Abbeel, P.: Denoising diffusion probabilistic models. NeurIPS (2020)
- 27. Hochreiter, S.: The vanishing gradient problem during learning recurrent neural nets and problem solutions. International Journal of Uncertainty, Fuzziness and Knowledge-Based Systems **6**(02), 107–116 (1998)
- 28. Howard, J.: A smaller subset of 10 easily classified classes from imagenet, and a little more french. URL https://github.com/fastai/imagenette (2019)
- Karras, T., Aittala, M., Laine, S., Härkönen, E., Hellsten, J., Lehtinen, J., Aila,
 T.: Alias-free generative adversarial networks. NeurIPS 34, 852–863 (2021)
- Karras, T., Laine, S., Aila, T.: A style-based generator architecture for generative adversarial networks. In: CVPR. pp. 4401–4410 (2019)
- 31. Katharopoulos, A., Fleuret, F.: Not all samples are created equal: Deep learning with importance sampling. In: ICML. pp. 2525–2534. PMLR (2018)
- 32. Kim, J.H., Kim, J., Oh, S.J., Yun, S., Song, H., Jeong, J., Ha, J.W., Song, H.O.: Dataset condensation via efficient synthetic-data parameterization. In: International Conference on Machine Learning. pp. 11102–11118. PMLR (2022)
- Krizhevsky, A., Sutskever, I., Hinton, G.E.: Imagenet classification with deep convolutional neural networks. Advances in neural information processing systems 25 (2012)
- Kwon, M., Jeong, J., Uh, Y.: Diffusion models already have a semantic latent space.
 arXiv preprint arXiv:2210.10960 (2022)
- 35. Li, H., Yang, Y., Chang, M., Chen, S., Feng, H., Xu, Z., Li, Q., Chen, Y.: Srdiff: Single image super-resolution with diffusion probabilistic models. Neurocomputing 479, 47–59 (2022)
- Liu, Y., Gu, J., Wang, K., Zhu, Z., Jiang, W., You, Y.: Dream: Efficient dataset distillation by representative matching. arXiv preprint arXiv:2302.14416 (2023)
- 37. Lugmayr, A., Danelljan, M., Romero, A., Yu, F., Timofte, R., Van Gool, L.: Repaint: Inpainting using denoising diffusion probabilistic models. In: Proceedings of the IEEE/CVF Conference on Computer Vision and Pattern Recognition. pp. 11461–11471 (2022)
- 38. Masarczyk, W., Tautkute, I.: Reducing catastrophic forgetting with learning on synthetic data. In: CVPR. pp. 252–253 (2020)
- Mirzasoleiman, B., Bilmes, J., Leskovec, J.: Coresets for data-efficient training of machine learning models. In: International Conference on Machine Learning. pp. 6950–6960. PMLR (2020)
- 40. Moser, B., Frolov, S., Raue, F., Palacio, S., Dengel, A.: Waving goodbye to low-res: A diffusion-wavelet approach for image super-resolution. arXiv preprint arXiv:2304.01994 (2023)
- 41. Moser, B., Raue, F., Hees, J., Dengel, A.: Less is more: Proxy datasets in nas approaches. In: CVPR. pp. 1953–1961 (2022)

- 42. Moser, B.B., Frolov, S., Raue, F., Palacio, S., Dengel, A.: Yoda: You only diffuse areas. an area-masked diffusion approach for image super-resolution. arXiv preprint arXiv:2308.07977 (2023)
- 43. Moser, B.B., Raue, F., Frolov, S., Palacio, S., Hees, J., Dengel, A.: Hitchhiker's guide to super-resolution: Introduction and recent advances. IEEE Transactions on Pattern Analysis and Machine Intelligence (2023)
- 44. Moser, B.B., Shanbhag, A.S., Raue, F., Frolov, S., Palacio, S., Dengel, A.: Diffusion models, image super-resolution and everything: A survey. arXiv preprint arXiv:2401.00736 (2024)
- 45. Mukhopadhyay, S., Gwilliam, M., Agarwal, V., Padmanabhan, N., Swaminathan, A., Hegde, S., Zhou, T., Shrivastava, A.: Diffusion models beat gans on image classification. arXiv preprint arXiv:2307.08702 (2023)
- 46. Müller-Franzes, G., Niehues, J.M., Khader, F., Arasteh, S.T., Haarburger, C., Kuhl, C., Wang, T., Han, T., Nebelung, S., Kather, J.N., et al.: Diffusion probabilistic models beat gans on medical images. arXiv preprint arXiv:2212.07501 (2022)
- 47. Namatevs, I., Sudars, K., Nikulins, A., Slaidina, A., Neimane, L., Radzins, O., Edelmers, E.: Denoising diffusion algorithm for single image inplaine superresolution in cbct scans of the mandible. In: 2023 IEEE 64th International Scientific Conference on Information Technology and Management Science of Riga Technical University (ITMS). pp. 1–6. IEEE (2023)
- 48. Nguyen, T., Chen, Z., Lee, J.: Dataset meta-learning from kernel ridge-regression. arXiv preprint arXiv:2011.00050 (2020)
- 49. Nguyen, T., Novak, R., Xiao, L., Lee, J.: Dataset distillation with infinitely wide convolutional networks. NeurIPS (2021)
- Nichol, A.Q., Dhariwal, P.: Improved denoising diffusion probabilistic models. PMLR (2021)
- 51. Park, Y.H., Kwon, M., Choi, J., Jo, J., Uh, Y.: Understanding the latent space of diffusion models through the lens of riemannian geometry. arXiv preprint arXiv:2307.12868 (2023)
- 52. Parmar, G., Li, Y., Lu, J., Zhang, R., Zhu, J.Y., Singh, K.K.: Spatially-adaptive multilayer selection for gan inversion and editing. In: CVPR. pp. 11399–11409 (2022)
- 53. Ramesh, A., Dhariwal, P., Nichol, A., Chu, C., Chen, M.: Hierarchical text-conditional image generation with clip latents. arXiv preprint arXiv:2204.06125 1(2), 3 (2022)
- 54. Ridnik, T., Ben-Baruch, E., Noy, A., Zelnik-Manor, L.: Imagenet-21k pretraining for the masses. arXiv preprint arXiv:2104.10972 (2021)
- 55. Rombach, R., Blattmann, A., Lorenz, D., Esser, P., Ommer, B.: High-resolution image synthesis with latent diffusion models. In: CVPR (2022)
- 56. Saharia, C., Ho, J., Chan, W., Salimans, T., Fleet, D.J., Norouzi, M.: Image super-resolution via iterative refinement. arXiv:2104.07636 (2021)
- 57. Saharia, C., Ho, J., Chan, W., Salimans, T., Fleet, D.J., Norouzi, M.: Image superresolution via iterative refinement. IEEE Transactions on Pattern Analysis and Machine Intelligence 45(4), 4713–4726 (2022)
- 58. Sauer, A., Schwarz, K., Geiger, A.: Stylegan-xl: Scaling stylegan to large diverse datasets. In: ACM SIGGRAPH 2022 conference proceedings. pp. 1–10 (2022)
- 59. Simonyan, K., Zisserman, A.: Very deep convolutional networks for large-scale image recognition. ICLR (2014)

- 60. Such, F.P., Rawal, A., Lehman, J., Stanley, K., Clune, J.: Generative teaching networks: Accelerating neural architecture search by learning to generate synthetic training data. In: ICML (2020)
- 61. Touvron, H., Lavril, T., Izacard, G., Martinet, X., Lachaux, M.A., Lacroix, T., Rozière, B., Goyal, N., Hambro, E., Azhar, F., et al.: Llama: Open and efficient foundation language models. arXiv preprint arXiv:2302.13971 (2023)
- 62. Tov, O., Alaluf, Y., Nitzan, Y., Patashnik, O., Cohen-Or, D.: Designing an encoder for stylegan image manipulation. ACM Transactions on Graphics (TOG) **40**(4), 1–14 (2021)
- 63. Wang, T., Zhu, J.Y., Torralba, A., Efros, A.A.: Dataset distillation. arXiv preprint arXiv:1811.10959 (2018)
- 64. Xia, W., Zhang, Y., Yang, Y., Xue, J.H., Zhou, B., Yang, M.H.: Gan inversion: A survey. IEEE Transactions on Pattern Analysis and Machine Intelligence **45**(3), 3121–3138 (2022)
- Yang, L., Zhang, Z., Song, Y., Hong, S., Xu, R., Zhao, Y., Zhang, W., Cui, B., Yang, M.H.: Diffusion models: A comprehensive survey of methods and applications. ACM Computing Surveys 56(4), 1–39 (2023)
- 66. Yu, T., Feng, R., Feng, R., Liu, J., Jin, X., Zeng, W., Chen, Z.: Inpaint anything: Segment anything meets image inpainting. arXiv preprint arXiv:2304.06790 (2023)
- 67. Zhao, B., Bilen, H.: Dataset condensation with differentiable siamese augmentation. In: ICML (2021)
- 68. Zhao, B., Bilen, H.: Dataset condensation with distribution matching. In: WACV (2023)
- 69. Zhao, B., Mopuri, K.R., Bilen, H.: Dataset condensation with gradient matching. ICLR (2020)
- Zheng, G., Zhou, X., Li, X., Qi, Z., Shan, Y., Li, X.: Layoutdiffusion: Controllable diffusion model for layout-to-image generation. In: CVPR. pp. 22490–22499 (June 2023)
- 71. Zhu, J.Y., Krähenbühl, P., Shechtman, E., Efros, A.A.: Generative visual manipulation on the natural image manifold. In: ECCV. pp. 597–613. Springer (2016)
- 72. Zhu, P., Abdal, R., Femiani, J., Wonka, P.: Barbershop: Gan-based image compositing using segmentation masks. arXiv preprint arXiv:2106.01505 (2021)
- 73. Zhu, P., Abdal, R., Qin, Y., Femiani, J., Wonka, P.: Improved stylegan embedding: Where are the good latents? arXiv preprint arXiv:2012.09036 (2020)

Supplementary Material

Hyper-Parameters for Distillation Algorithms

Parameter	Value
DSA Augmentations	Color / Crop / Cutout / Flip / Scale / Rotate
Iteration (Distillation)	$5{,}000~(128 \times 128)~/~10{,}000~(256 \times 256$
Momentum	0.5
Batch Real	256
Batch Train	256
Batch Test	128

LDM. For all our LDM experiments, we set the unconditional guidance scale to default value 3. For 128×128 images, we used max. time steps of 10, and for 256×256 images, we used 20.

DC. We utilize a learning rate of 10^{-3} throughout our DC experiments to update the latent code representation and the conditioning information.

DM. In every DM experiment conducted, we adopt a learning rate of 10^{-2} , applying it to updates of the latent code representation alongside the conditioning information.

MTT. For MTT experiments, a uniform learning rate of 10 is applied to update the latent code representation and the conditioning information. We buffered 5,000 trajectories for expert training, each with 15 training epochs. We used ConvNet-5 and InstanceNorm. During dataset distillation, we used three expert epochs, max. start epoch of 5 and 20 synthetic steps.

Classes in Subsets

Table 5 list ImageNet classes that are used in the subsets employed in this work.

Dataset	0	1	2	3	4	5	6	7	8	9
ImageNet-A	Leonberg	Probiscis Monkey	Rapeseed	Three-Toed Sloth	Cliff Dwelling	Yellow Lady's Slipper	Hamster	Gondola	Orca	Limpkin
ImageNet-B	Spoonbill	Website	Lorikeet	Hyena	Earthstar	Trollybus	Echidna	Pomeranian	Odometer	Ruddy Turnstone
ImageNet-C	Freight Car	Hummingbird	Fireboat	Disk Brake	Bee Eater	Rock Beauty	Lion	European Gallinule	Cabbage Butterfly	Goldfinch
ImageNet-D	Ostrich	Samoyed	Snowbird	Brabancon Griffon	Chickadee	Sorrel	Admiral	Great Gray Owl	Hornbill	Ringlet
ImageNet-E	Spindle	Toucan	Black Swan	King Penguin	Potter's Wheel	Photocopier	Screw	Tarantula	Sscilloscope	Lycaenid
ImageNette	Tench	English Springer	Cassette Player	Chainsaw	Church	French Horn	Garbage Truck	Gas Pump	Golf Ball	Parachute
ImageWoof	Australian Terrier	Border Terrier	Samoyed	Beagle	Shih-Tzu	English Foxhound	Rhodesian Ridgeback	Dingo	Golden Retriever	English Sheepdog
ImageNet-Birds	Peacock	Flamingo	Macaw	Pelican	King Penguin	Bald Eagle	Toucan	Ostrich	Black Swan	Cockatoo
ImageNet-Fruits	Pineapple	Banana	Strawberry	Orange	Lemon	Pomegranate	Fig	Bell Pepper	Cucumber	Granny Smith Apple
ImageNet-Cats	Tabby Cat	Bengal Cat	Persian Cat	Siamese Cat	Egyptian Cat	Lion	Tiger	Jaguar	Snow Leonard	Lynx

Table 5: Class listings for our ImageNet subsets.

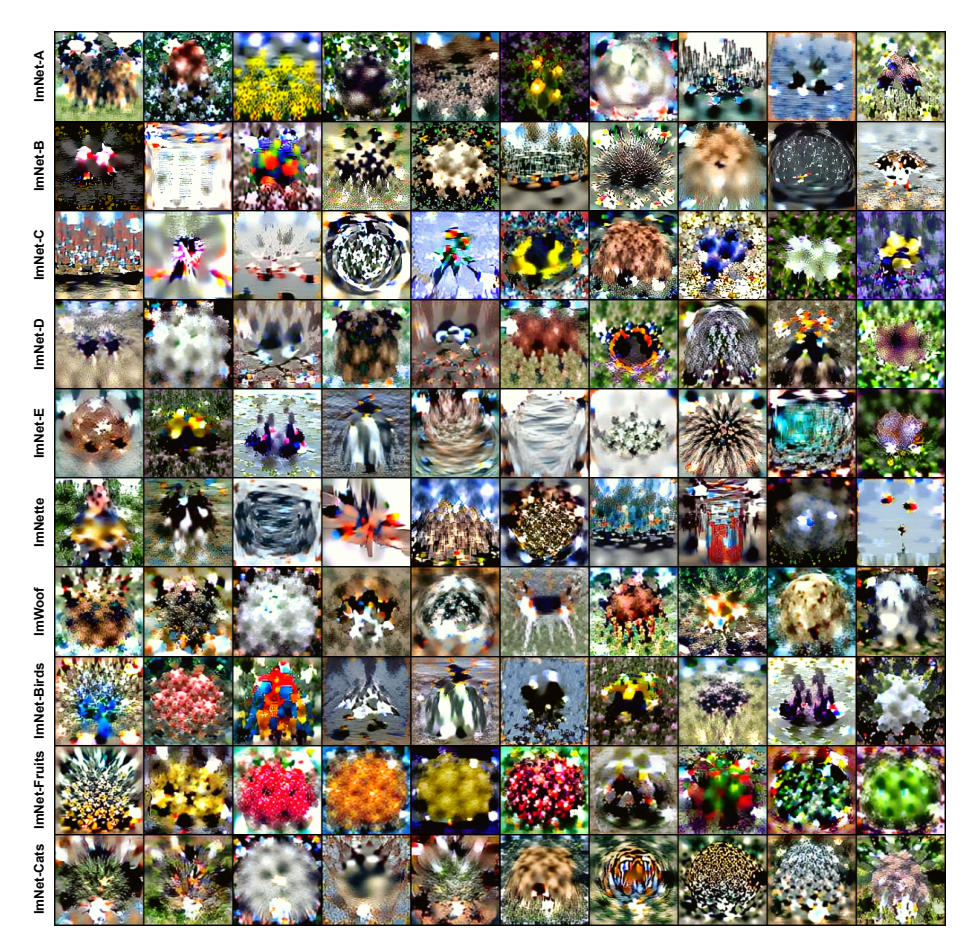


Fig. 6: Images distilled by MTT in LD3M for IPC=1.



Fig. 7: Images distilled by DC in LD3M for IPC=1.

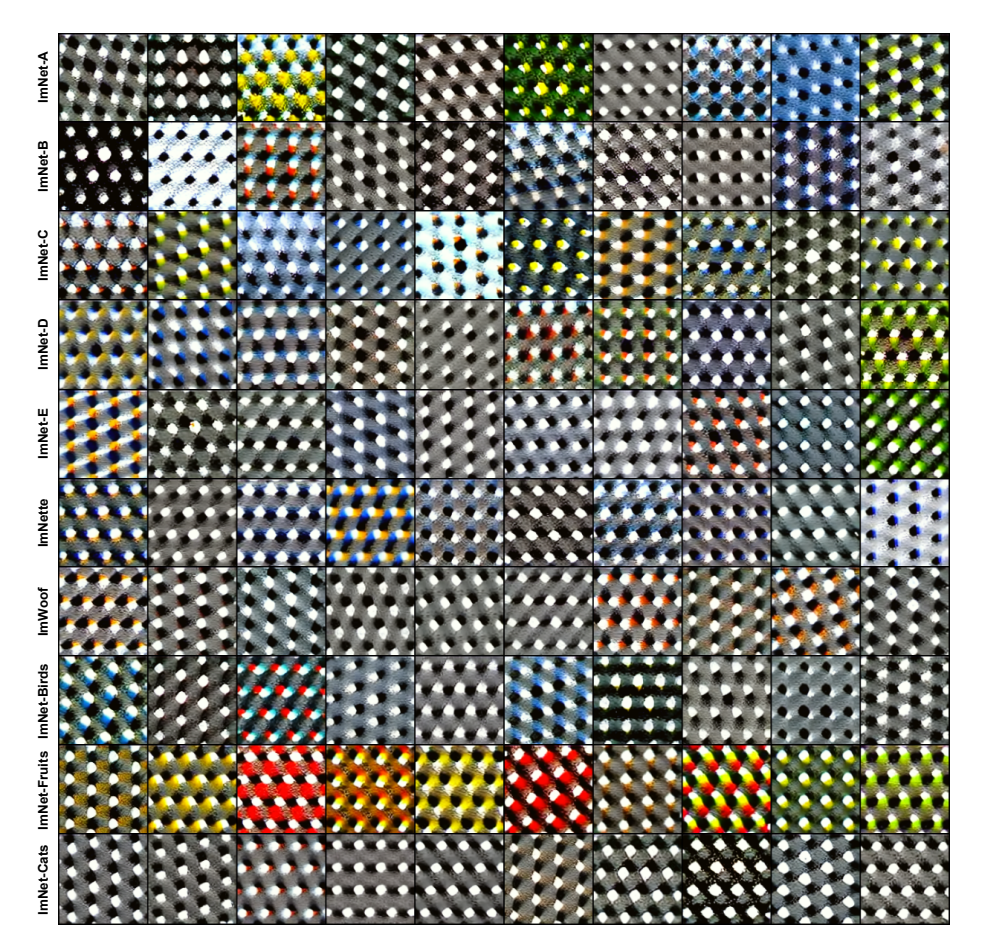


Fig. 8: Images distilled by DM in LD3M for IPC=1.



Fig. 9: Images distilled by DC in LD3M for IPC=10 and ImageNet-A.



Fig. 10: Images distilled by DC in LD3M for IPC=10 and ImageNet-B.



Fig. 11: Images distilled by DC in LD3M for IPC=10 and ImageNet-C.

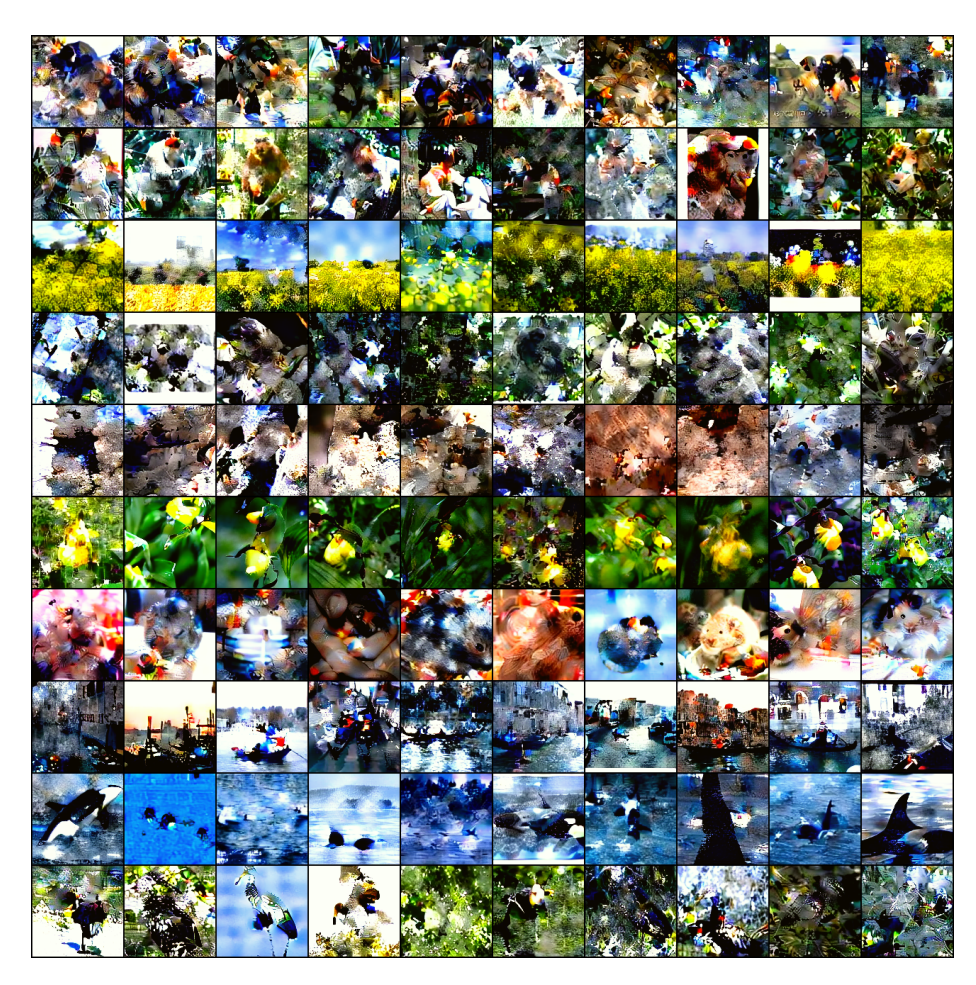


Fig. 12: Images distilled by DM in LD3M for IPC=10 and ImageNet-A.

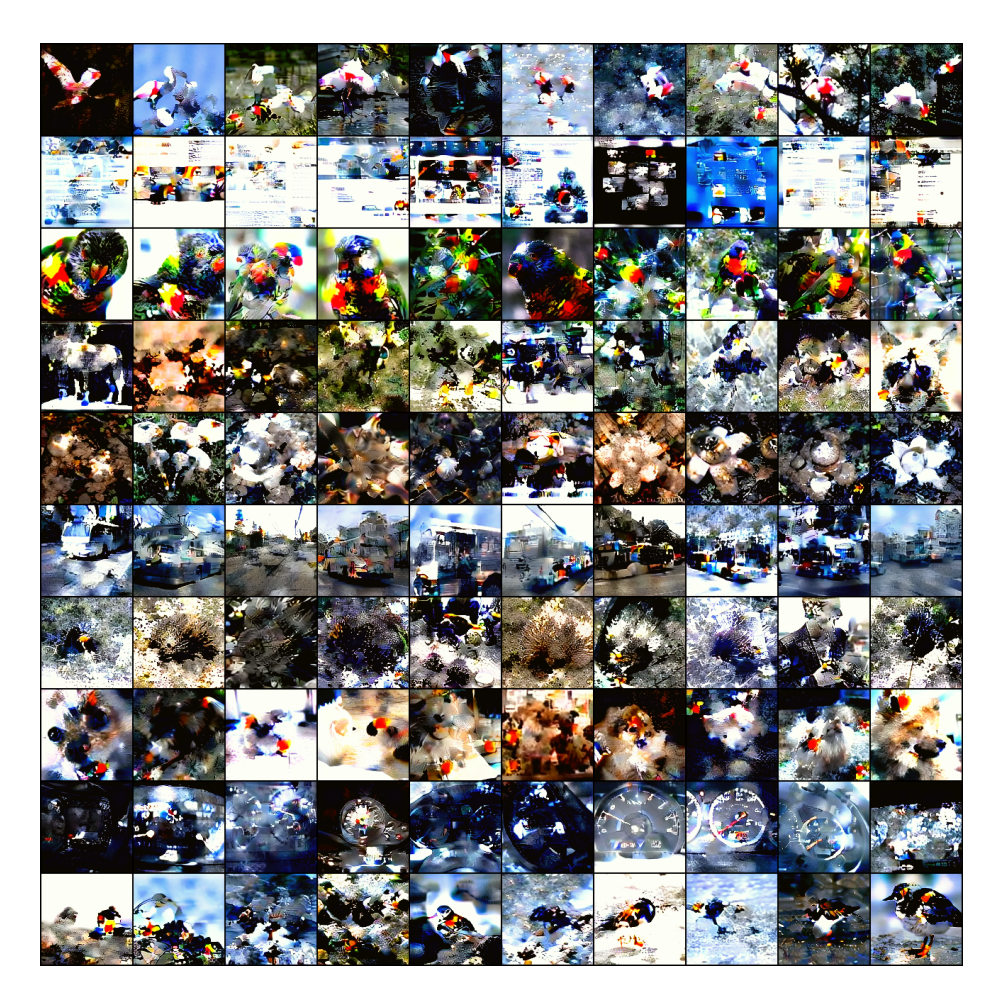


Fig. 13: Images distilled by DM in LD3M for IPC=10 and ImageNet-B.

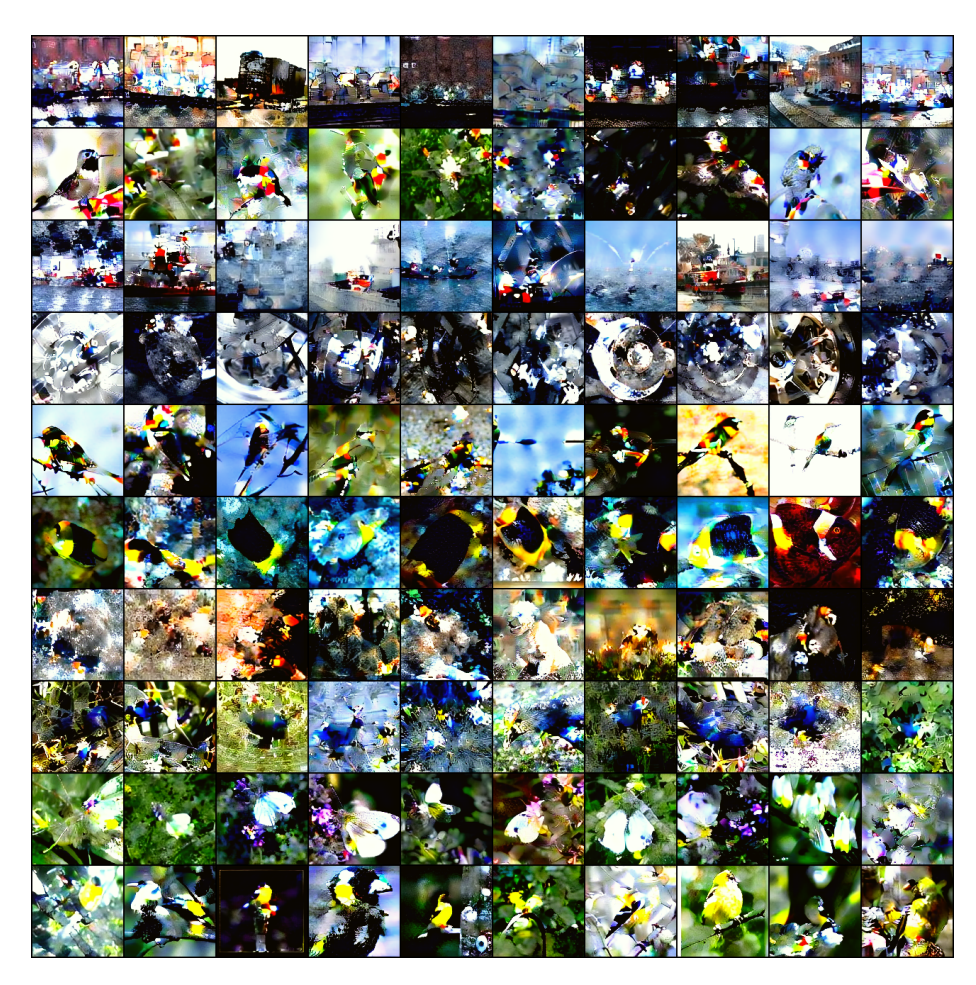


Fig. 14: Images distilled by DM in LD3M for IPC=10 and ImageNet-C.

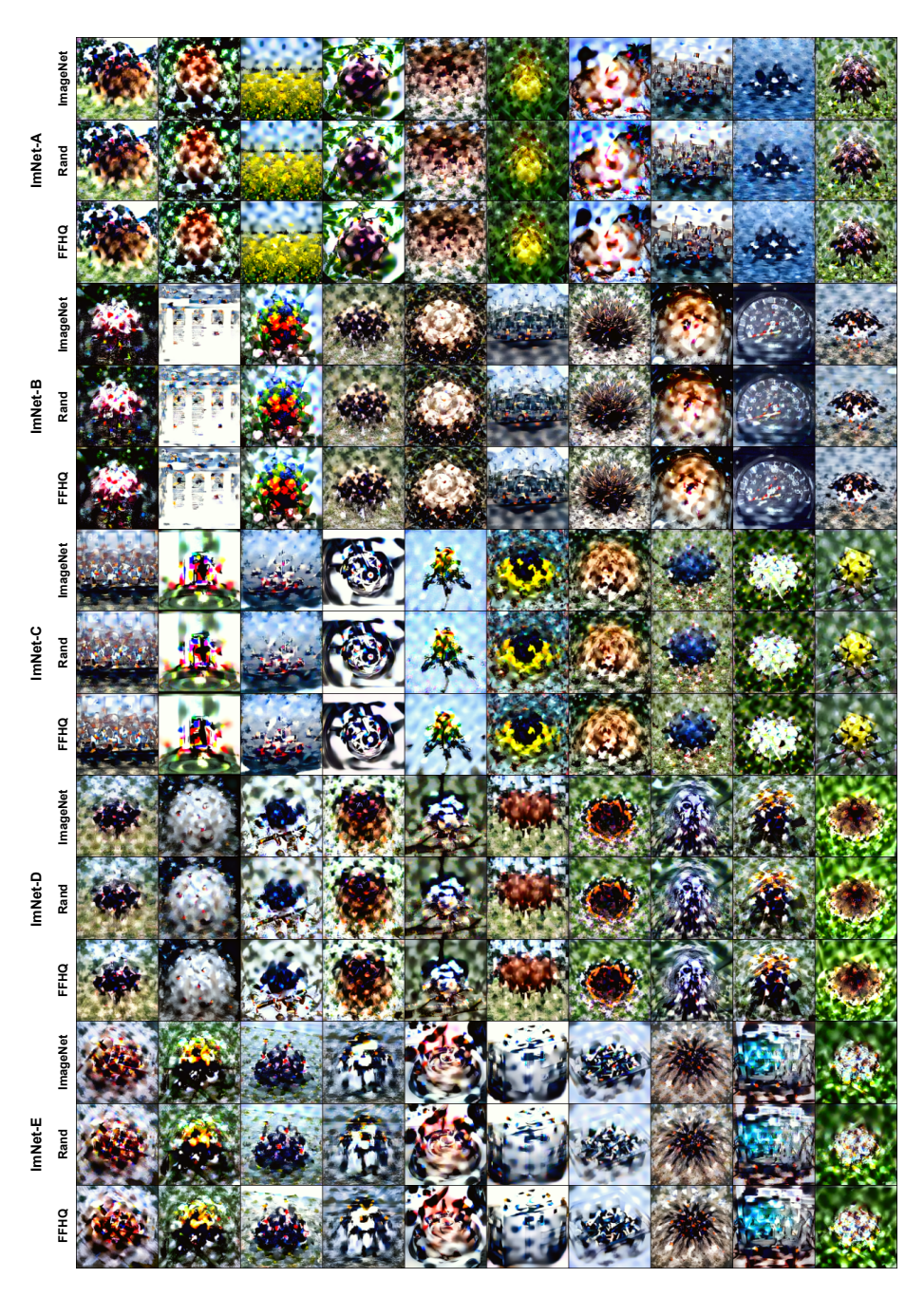


Fig. 15: Comparison of 256×256 distilled images with differently trained LDMs (ImageNet, FFHQ, and random).